Journal of Alloys and Compounds 888 (2021) 161452

Contents lists available at ScienceDirect

Journal of Alloys and Compounds

journal homepage: www.elsevier.com/locate/jalcom

Effect of nitrogen on microstructure and mechanical properties of the CoCrFeMnNi high-entropy alloy after cold rolling and subsequent annealing

A. Semenyuk*, M. Klimova, D. Shaysultanov, G. Salishchev, S. Zherebtsov, N. Stepanov

Laboratory of Bulk Nanostructured Materials, Belgorod State University, Belgorod 308015, Russia

ARTICLE INFO

Article history:
Received 4 June 2021
Received in revised form 26 July 2021
Accepted 3 August 2021
Available online 5 August 2021

Keywords:
High-entropy alloys
Microstructure
Mechanical properties
Electron microscopy

ABSTRACT

The effect of nitrogen on the structure and mechanical behavior of a CoCrFeMnNi high-entropy alloy after rolling and subsequent annealing was examined. The as-cast alloys doped with 0.5, 1.0, and 2.0 at% N were cold rolled to 80% thickness reduction. Further annealing in the temperature range of 700–1000 °C for 1 h has resulted in (i) development of recrystallization in the fcc matrix and (ii) precipitation of the M_2N type nitrides in the alloys with 1.0 and 2.0 at% N. The recrystallization onset temperature lowered with an increase in the N content. Besides, the fcc grain size in the alloy with 2.0 at% N was considerably smaller than that in the alloys with a lower nitrogen content due to a strong pinning effect of the nitride particles. The cold-rolled alloys had high strength, but very limited ductility. The recrystallized microstructure has resulted in a much better strength-ductility synergy when tested at 293 K. For example, the alloy with 2.0 at % N after annealing at 900 °C had the yield strength of 673 MPa, ultimate tensile strength of 1021 MPa, and ductility of 47%. A decrease in the testing temperature to 77 K has resulted in a considerable increase in strength. For example, the same alloy had the yield strength and ultimate tensile strength of 1097 and 1548 MPa, respectively. The quantitative analysis of the strengthening mechanisms has revealed that (i) grain boundary strengthening provides the highest contribution at 293 K (ii) the increase in strength at 77 K is mostly associated with the lattice friction and interstitial solid solution hardening.

1. Introduction

The first works on the so-called high-entropy alloys (HEAs) date back to 2004 and belong to Yeh et al. [1]. In their works, they reported the possibility of obtaining single-phase structures in complex alloys consisting of 5 or more elements, taken in equal proportions. Since then, many scientists have become interested in the development and research of HEAs due to their unusual structures and attractive properties, including high strength, ductility, hardness, fracture toughness, etc. [2–5]. Currently, many HEAs are considered as promising structural materials; for example, alloys consisting of refractory elements have attractive high-temperature strength and can potentially be used in the aerospace industry [6–9].

One of the most well-studied HEAs classes is alloys with a face-centered cubic (fcc) lattice based on the Co-Cr-Fe-Ni-Mn system [10–13]. The equiatomic CoCrFeMnNi alloy was initially developed by Cantor et al. [10]. The CoCrFeMnNi alloy has high ductility and fracture toughness both at room and cryogenic temperatures. The impressive cryogenic properties are usually attributed to the development of nano-twinning [3,13]. Currently, derivatives of the Cantor alloy with improved properties are being created. For example, the equiatomic CoCrNi alloy has even better strength and toughness at cryogenic temperature in comparison with the Cantor alloy [13–15]. However, fcc alloys of the Co-Cr-Fe-Mn-Ni system have mostly a relatively low yield strength at room temperature [16–18].

One of the ways to improve strength of the fcc HEAs is associated with doping with interstitial elements [19–28]. For example, extensive efforts were devoted to studies of carbon-doped alloys. It has been found that the addition of even a small amount of carbon can significantly increase strength without loss of ductility [22,24,25]. An increase in strength is associated with either interstitial solid solution strengthening or precipitation (due to the formation of the carbide) strengthening. Carbon also affects the contribution of various deformation mechanisms (dislocation slip and twinning), although contradictory observations are available in the literature [23,26–31]. Most possibly, the effect of interstitials on deformation mechanisms

* Correspondence to: Laboratory of Bulk Nanostructured Materials, Belgorod National Research University, Pobeda 85, Belgorod 308015, Russia.
E-mail address: semenyuk@bsu.edu.ru (A. Semenyuk).

https://doi.org/10.1016/j.jallcom.2021.161452
0925-8388/

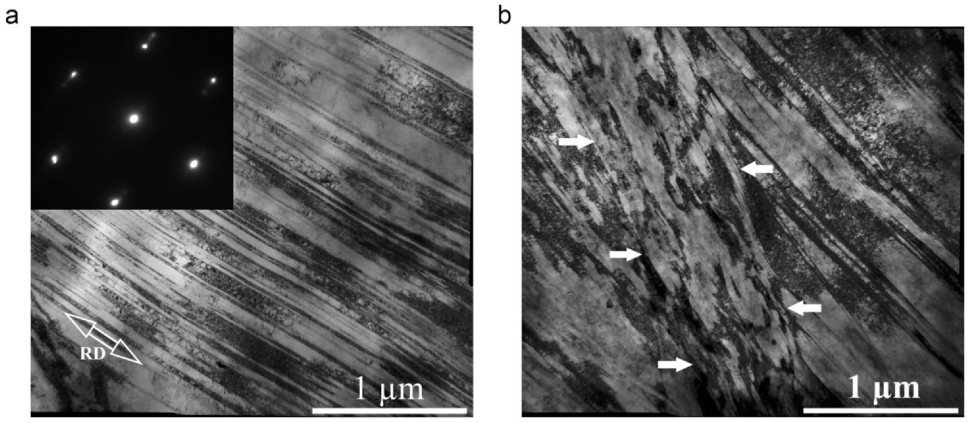

Fig. 1. TEM bright field images of the $CoCrFeMnNiN_x$ alloys with x = 0.5 (a) and 2.0 (b) after cold rolling to 80% thickness reduction. Rolling direction (RD) is indicated with arrow in (a). Shear band is indicated with white arrows in (b).

strongly depends on the exact chemical composition of the matrix phase. At the same time, the influence of other interstitial elements, in particular, nitrogen, on the structure and mechanical properties of the Co-Cr-Fe-Mn-Ni system alloys is rather poorly studied [32–45].

Another approach to increase strength of HEAs is thermomechanical processing. Due to a strong temperature sensitivity, the Hall-Petch coefficient in Cantor-type alloys becomes high at room and cryogenic temperatures [3,24,52]. Thus, the formation of a fine-grained recrystallized structure is a promising way of obtaining a good strength-ductility synergy [36,37]. It should be noted that second phase particles, including carbides [30,38], can prevent growth of the fcc grains. However, although some reports on the structure and properties of thermomechanically processed nitrogen-doped fcc HEAs has been published [39–42], there is no comprehensive understanding of the composition-structure-properties relationships in such alloys. Earlier, we have investigated the structure and mechanical properties of as-cast equiatomic CoCrFeMnNi alloys with different nitrogen contents [43]. In a continuation of that work, we have performed cold rolling with subsequent annealing of the same alloys. Here, we report the obtained cold-worked and recrystallized structures and room and cryogenic temperature mechanical properties of the nitrogen-doped CoCrFeMnNi alloys.

2. Materials and methods

The equiatomic high entropy CoCrFeMnNi alloys with different amounts of nitrogen (the nominal percentages were 0.5, 1.0, and 2.0 at%) were produced by induction melting of the pure components in high-purity argon with subsequent casting. Nitrogen was added in the form of ferrochrome nitride. The obtained ingots had dimensions of about 65 × 40 × 20 mm^2. The concentrations of the principal elements were determined by energy dispersive spectrometry (EDS) analysis; the concentration of nitrogen was determined by LECO thermal-combustion analysis. The measured chemical composition of the alloy is shown in Table 1. Rectangular-shaped specimens with a thickness of 8 mm were cut from the ingot by an electric discharge machine. The samples were then rolled in several passes at room temperature until the thickness was reduced by 80% (from 8 to 1.6 mm). The reduction per each pass was 5–10%. After rolling, the samples were cut from the plate and annealed in a muffle furnace in an air atmosphere at 700–1000 °C for 1 h, followed by air cooling. The annealing conditions were selected following the literature data on thermomechanically processed interstitial fcc HEAs to obtain a recrystallized fcc matrix with different grain sizes [3,27,40,42,44,51].

Table 1
Measured chemical composition of the program alloys depending on the nitrogen content.

Nitrogen content, at% (x)	Concentration of the elements, at%					
	Co	Cr	Fe	Mn	Ni	N
0.5	20.10	20.10	19.61	19.80	19.94	0.45
1.0	19.81	20.05	19.71	19.54	20.01	0.88
2.0	19.61	19.71	19.43	19.46	19.60	2.19

The structure of the alloy was studied using scanning (SEM) and transmission (TEM) electron microscopy in the RD-ND plane (perpendicular to the transversal direction). XRD analysis was performed using a RIGAKU diffractometer with Cu K-α irradiation. SEM studies were carried out using a FEI Quanta 600 FEG microscope equipped with a backscattered electron (BSE) detector. Samples for SEM observations were mechanically polished with different SiC papers and a colloidal silica suspension. TEM investigations were conducted using a JEOL JEM-2100 microscope with an accelerating voltage of 200 kV equipped with an EDS detector. Selected area electron diffraction (SAED) patterns were used for the phase identification; the results of EDS were used for chemical analysis. Samples for TEM analysis were prepared by conventional twin-jet electro-polishing of mechanically pre-thinned to 100 μm foils, in a mixture of 90% CH3COOH and 10% HClO4 at the 27 V potential at room temperature. The size/fractions of recrystallized grains and size/number of precipitates were quantified using at least 10 SEM or TEM images with a low magnification. On average, ~500 grains were analyzed per each condition to get the average grain size.

Tensile tests were carried out using Instron 5882 universal tensile testing machine with a strain rate of 1×10^{-3} s^{-1} at room (293 K) and cryogenic (77 K) temperatures using samples with the gage measured 6 × 3 × 1.5 mm^3. The samples were cut from the annealed sheets by electrical discharge machine and carefully mechanically polished. For cryogenic testing, the test specimen and both grips are held in an open-top vessel filled with liquid nitrogen before the test starting to equilibrate the temperature. Elongation to fracture was determined by measuring the spacing between marks designating the gauge length before and after the test. At least 3 specimens were tested per condition.

3. Results

3.1. Microstructure

The as-cast structures of the program alloys were reported elsewhere [49], therefore only brief information is presented here.

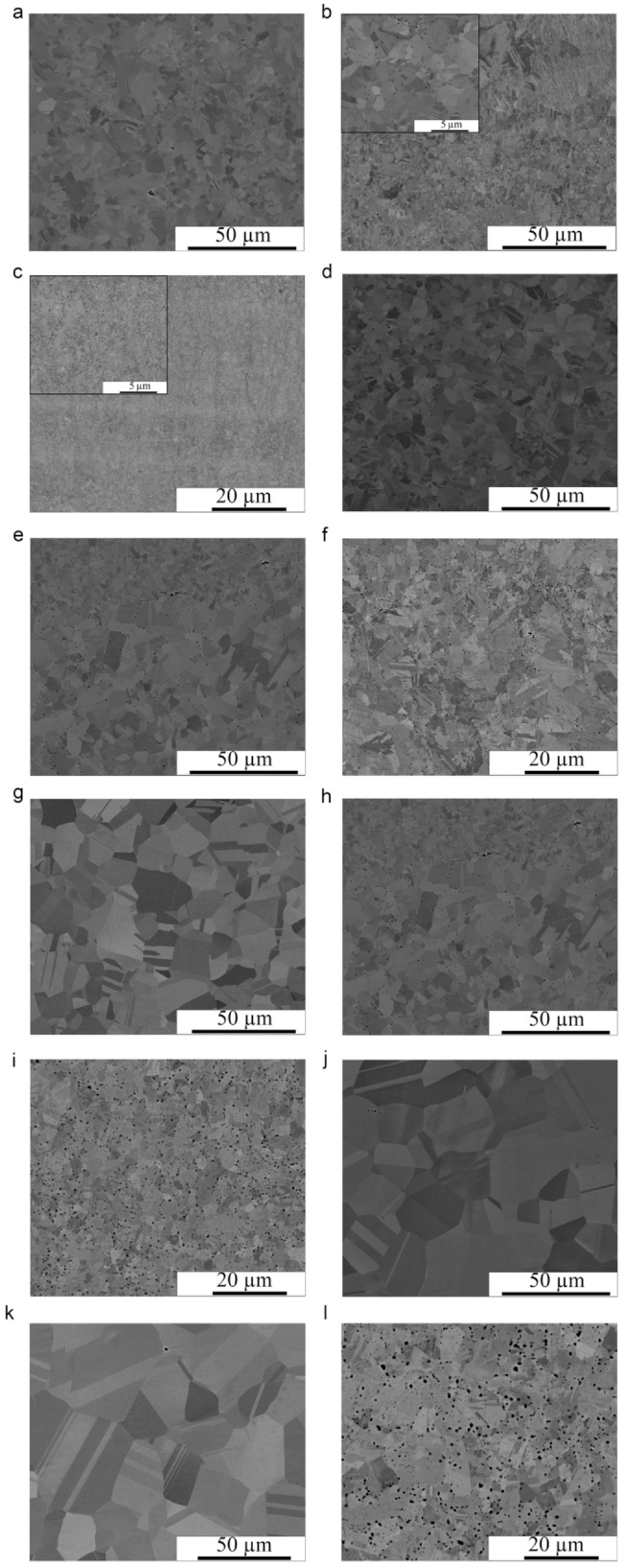

Fig. 2. SEM-BSE images of the microstructure of the CoCrFeNiMn alloys with different nitrogen contents (x): x = 0.5 (a, d, g, j); 1.0 (b, e, h, k); 2.0 (c, f, i, l) after annealing at 700 °C (a-c); 800 °C (d-f); 900 °C (g-i); 1000 °C (j-l).

The x = 0.5 and x = 1.0 alloys had a single fcc phase coarse-grained microstructure, while in the x = 2.0 alloy a small portion of fine Cr-rich M_2N type nitrides was found predominantly at grain boundaries.

Fig. 1 shows TEM images of the x = 0.5 and x = 2.0 alloys after cold rolling. Cold deformation produced a lamellar structure aligned with the rolling direction. Note that no signs of deformation twins were found (see SAED in Fig. 1a for example). In turn, some shear bands can be observed (see Fig. 1b for example). Significant dislocation density can also be noted. At the same time, there was no noticeable difference in the microstructure of the alloys with different nitrogen content. It should be noted that no M_2N precipitates were observed in the deformed x = 2.0 alloy, possibly due to their low fraction and significant density of defects that can mask the presence of the second phase particles.

The annealed microstructures of the alloys are first illustrated with SEM images in Fig. 2. Quantitative information on the microstructure, including grain size and fraction, and size of precipitates are collected in Table 2. The response of microstructure to annealing strongly depended both on temperature and alloys composition. For instance, a fully recrystallized microstructure with the grain size of 3.1 μm was observed in the x = 0.5 alloy after annealing at 700 °C (Fig. 2a). An increase in the N content has hindered the development of recrystallization processes. For example, in the x = 1.0 alloy the recrystallized volume fraction was only 56%. The respective average recrystallized grain size was 1.8 μm. In turn, a completely uncrystallized structure was found in the x = 2.0 alloy by SEM studies (Fig. 2c). Note that some dark precipitates were found both in the x = 1.0 and x = 2.0 alloys (see high magnification inserts in Fig. 2b and c).

An increase in the annealing temperature to 800 °C has resulted in some coarsening of the recrystallized grains in the x = 0.5 alloy. The average grain size approached 4.4 μm. Numerous annealing twins were observed. A fully recrystallized microstructure with a mean grain size of 5.4 μm was observed in the x = 1 alloy (Fig. 2e). In addition, numerous dark particles of secondary phase(s) were found. The x = 2.0 alloy was partially recrystallized after annealing at 800°C (Fig. 2f). The volume fraction of the recrystallized areas was 69%. Many secondary phase(s) particles were found predominantly in the recrystallized areas.

After annealing at 900 and 1000 °C, a fully recrystallized structure was found in all the program alloys (Fig. 2g-l). The recrystallized grain size increased with annealing temperature. However, the x = 2.0 alloy had a much finer structure in comparison with the alloys with lower nitrogen contents. Another important observation was associated with the secondary phases. A very small amount of the particles was found in the x = 1.0 alloy after annealing at 900 °C, and no particles were detected after annealing at 1000 °C (Fig. 2k). Meanwhile, plenty of particles were found in the x = 2.0 alloy after annealing at both temperatures (Fig. 2i, l) (Fig. 3).

Due to limited information obtained by the SEM method, TEM studies of the x = 2.0 alloy after annealing at 700°C were performed (Fig. 4). The majority of structure was unrecrystallized (Fig. 4a). However, apparent recovery and associated dislocations rearrangement took place during the annealing (compare Fig. 4a and Fig. 1b). Meanwhile, some areas of a recrystallized structure were observed (Fig. 4b); their estimated fraction was 15%. The average size of the recrystallized grains was 680 nm. Probably, the recrystallized areas were not visible clearly in the SEM images due to their low fraction and/or a fine size of the grains. Besides, numerous secondary phase precipitates were found in the recrystallized areas. The volume fraction and the mean size of the particles were 5.4% and 55 nm,

Table 2
Structural parameters (grain size, fraction, and size of secondary phases) of the CoCrFeNiMn alloys with different nitrogen contents (x) after annealing at temperatures of 700–1000 °C, following SEM-BSE data.

Annealing temperature, °C	x = 0.5	x = 1.0			x = 2.0		
	Grain size, μm	Grain size, μm	Particle size, nm	Volume fraction, %	Grain size, μm	Particle size, nm	Volume fraction, %
700	3.1 ± 1.8	1.8 ± 0.9	95 ± 35	1.9	0.7 ± 0.3[a]	55 ± 15[a]	5.4[a]
800	4.4 ± 2.2	5.4 ± 1.4	130 ± 50	1.5	1.3 ± 0.5	115 ± 45	9.1
900	10.5 ± 4.5	9.8 ± 3.4	150 ± 65	1.2	2.7 ± 0.8	165 ± 50	8.5
1000	19.4 ± 8.9	21.0 ± 11.3	–	–	4.2 ± 1.5	270 ± 80	5.8

[a] The data was obtained from TEM images (Fig. 4).

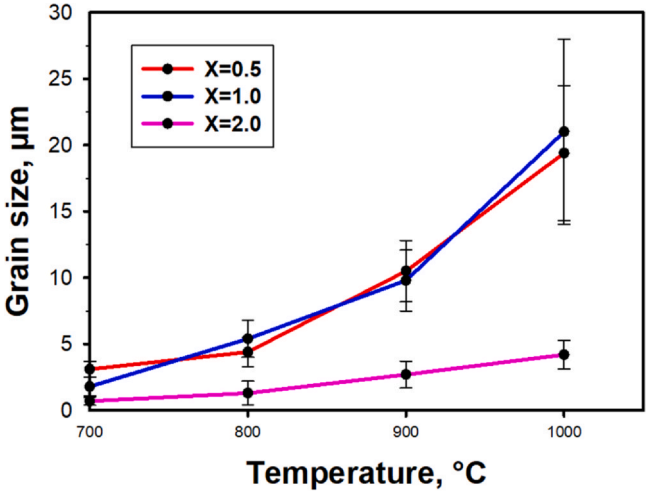

Fig. 3. Dependence of grain size on annealing temperature for the CoCrFeMnNi alloys with different N contents (x).

respectively. An analysis of selected area electron diffraction (SAED) patterns has shown that the particles were M_2N type nitrides. In turn, EDX has revealed that the nitrides were mostly composed of Cr (~70 at%; note that the resolution of the EDX system used in the present study was insufficient to determine reliably the content of light elements, like nitrogen, therefore only data for metallic elements was obtained). The formation of the Cr-rich M_2N particles in similar alloys has been already reported many times [32,39,40,43,44,55] and can be attributed to high affinity of N atoms to Cr [32,55]. The unrecrystallized areas did not contain any noticeable amount of the nitride particles.

To obtain more detailed information regarding the precipitated particles, XRD analysis and TEM investigations of the program alloys annealed at 900 °C were performed (Fig. 5a). XRD patterns (Fig. 5a) have revealed a dominant fcc phase with the lattice parameter of 3.615 ± 0.002 nm in all the alloys. In addition, peaks corresponding to the M_2N-type nitrides were detected in the x = 2.0 alloy. TEM investigations confirmed the absence of the secondary phase(s) in the x = 0.5 alloy (Fig. 5b). A small amount (1.2%) of second phase particles, identified by SAED as the M_2N nitrides, were observed in the x = 1 alloy (Fig. 5c). The amount of nitrides was probably lower than the XRD sensitivity limit. With an increase in the nitrogen concentration to 2 at%, both the size and the fraction of the nitrides increased to 110 nm and 9.3%, respectively.

3.2. Mechanical properties

To access the mechanical properties of the program alloys in different conditions, tensile tests at room temperature were performed. The obtained stress-strain curves are presented in Fig. 6, and the resulting mechanical properties (yield strength (YS), ultimate tensile strength (UTS), uniform elongation (UE), and total elongation (TE)) are given in Table 4. The cold-rolled alloys had high strength, but very limited strain hardening capacity and ductility. At the same time, strength of the cold-worked alloys increased with increasing nitrogen concentration, for example, the yield strength of the x = 0.5 alloy was 1212 MPa, while strength of the x = 2.0 alloy increased to 1487 MPa.

Post-deformation annealing resulted in the anticipated softening and an increase in ductility of the program alloys, yet the response depended strongly on the nitrogen content. Annealing of the x = 0.5 and x = 1.0 alloys at relatively low temperatures of 700–800 °C resulted in a very pronounced increase in ductility (total elongation ≥ 45%) and at least a twofold decrease in the yield strength in comparison with those of the cold-rolled condition. In turn, the x = 2.0 alloy showed much lower ductility (16–24%) but a quite high yield strength (726–985 MPa) after annealing at the same temperatures. Further decrease in the annealing temperature to 900–1000 °C resulted in high ductility of 42–69% in all the alloys. However, even after annealing at high temperatures strength increased proportionally with the nitrogen content.

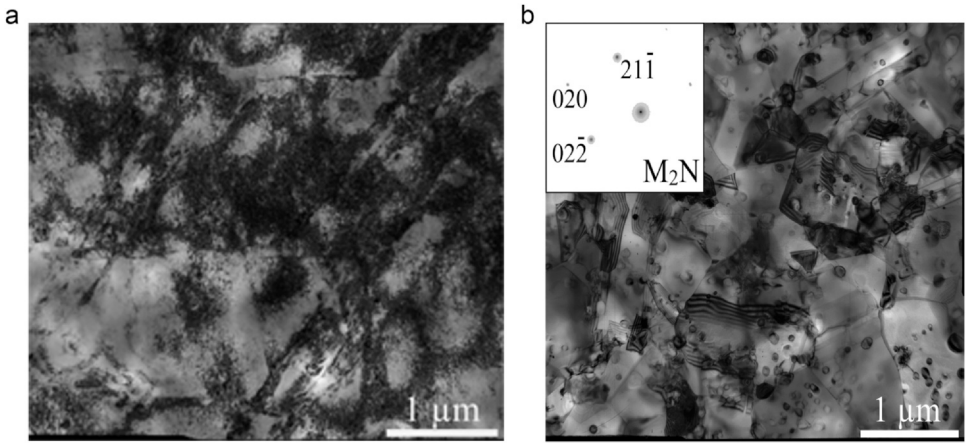

Fig. 4. TEM bright field images of the CoCrFeMnNi alloy with 2.0 at% of N after cold rolling and annealing at 700 °C for 1 h.

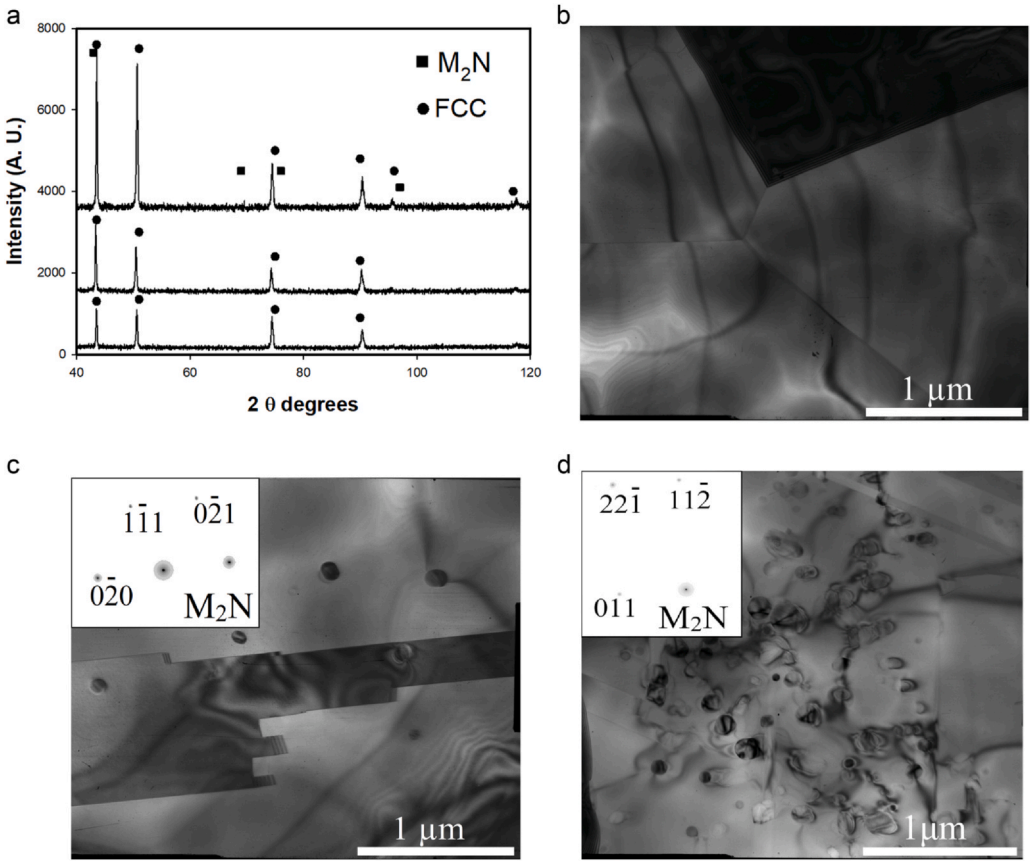

Fig. 5. XRD patterns (a) and TEM bright-field images of the CoCrFeMnNi alloys with x = 0.5 (b); x = 1.0 (c); x = 2.0 (d) after annealing at 900 °C for 1 h.

To gain further insights into the mechanical behavior of the program alloys, tensile tests of samples annealed at 800 and 900 °C were performed at 77 K. The obtained stress-strain curves and resulting mechanical properties are shown in Fig. 7 and Table 5, respectively. A decrease in the testing temperature has resulted in a pronounced increase in strength of the program alloys. An increase in the annealing temperature from 800 to 900 °C resulted in some softening of the alloys. Besides, the alloys became noticeably stronger with an increase in the nitrogen content. However, the effect of the testing temperature on ductility of the alloys was more complex. The x = 0.5 alloy became more ductile at 77 K. Ductility of the x = 1.0 alloy was barely affected by variations in the testing temperature. Meanwhile, ductility of the x = 2.0 alloy after annealing at 900 °C decreased in comparison with the room temperature testing. Note that in all conditions and testing temperatures ductility was inversely proportional to the nitrogen content.

The strain hardening curves of the CoCrFeMnNi alloys with different nitrogen contents after annealing at 900 °C obtained during tension at room or cryogenic temperatures are shown in Fig. 8. The alloys demonstrated qualitatively similar behavior irrespective of the nitrogen contents or testing temperatures. The strain hardening rate of the alloys was maximum at the initial stages of deformation and then decreased gradually until a rapid drop occurred at the final stages of deformation. The strain hardening rate at the initial stages of deformation was higher in the alloys with a higher nitrogen concentration. However, after a true strain of ~0.15–0.30, the hardening rate became inversely proportional to the nitrogen content. In addition, the strain hardening capacity improved at cryogenic temperatures. The strain-hardening curves for other conditions are not shown because they exhibit qualitatively similar behavior.

Fig. 9. shows TEM structures of the x = 2.0 alloy annealed at 900°C after tensile testing to 15% strain at 293 K and 77 K. Plastic deformation at room temperature was associated with intense dislocation sliding and the formation of diffuse dislocation pile-ups (Fig. 9a). Some sharp straight slip bands were also detected (see the central part of the image for the example), they were an indication of the development of planar slip in accordance with some earlier results on the same alloy in the as-cast condition [43]. A decrease in the testing temperature to 77 K led to an appearance of deformation twins, as is evident from SAED in Fig. 9b. The deformation twins were generally thin and straight. Besides, dislocation pile-ups were also observed in the microstructure after deformation at 77 K.

Table 3
Structure parameters (grain size, fraction, and size of secondary phases) of the CoCrFeNiMn alloys with different nitrogen contents (x) after annealing at 900 °C; particle size and volume fraction was evaluated using TEM.

Annealing temperature, °C	x = 0.5	x = 1.0			x = 2.0		
	Grain size, μm	Grain size, μm	Particle size, nm	Volume fraction, %	Grain size, μm	Particle size, μm	Volume fraction, %
900	10.5 ± 4.5	9.8 ± 3.4	150 ± 65	1.2	2.7 ± 0.8	110 ± 35	9.3

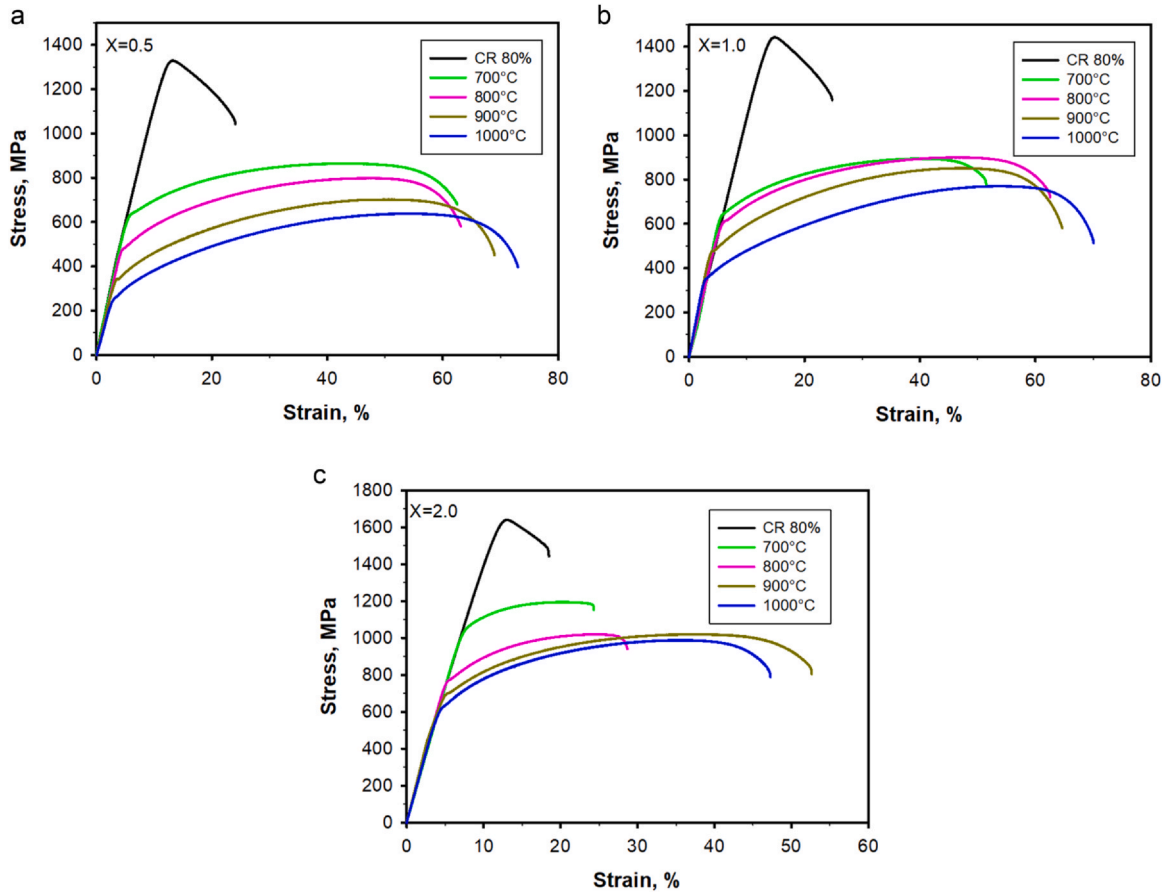

Fig. 6. Room temperature tensile stress-strain curves of the CoCrFeMnNi alloys with x = 0.5 (a), 1.0 (b), 2.0 (c) after cold rolling and 1 h annealing at different temperatures.

4. Discussion

The obtained results have demonstrated a pronounced dependence of both structure and mechanical properties of the recrystallized CoCrFeMnNi-based alloys on the nitrogen content and temperature of annealing. One of the most pronounced effects of the alloys conditions was associated with the precipitation of the Cr-rich M_2N nitride particles. No signs of the particles were detected in the x = 0.5 alloy, while 1–2% and 5–9% of particles were found in the x = 1.0 and x = 2.0 alloys, respectively (Table 2). Besides, no nitrides were detected in the x = 1.0 alloy after annealing at 1000 C, while plenty of particles were found in the x = 2.0 alloy after the same annealing treatment. Note that no particles were found in the as-cast both x = 0.5 and x = 1.0 alloys, and a small (~1%) amount of the nitrides were detected in the x = 2.0 alloy [43], i.e. the particles appeared (mostly) after heat treatment. Note also that the absence of the nitrides in the cold-worked and annealed CoCrFeMnNi-based alloys with ~0.5 at% N and precipitation of the M_2N particles in the alloys with the N content of ≥1.0 at% is in reasonable agreement with the available literature data [35,40,44,45].

Analysis of the results obtained in the current study suggests that (i) solubility of N in the fcc CoCrFeMnNi alloy is in the range of 0.5–1.0 at% N at 700–900 °C and > 1 at% at 1000 °C; (ii) the solvus temperature of the M_2N particles is in range 900–1000 °C and > 1000°C in the x = 1.0 and x = 2.0 alloys, respectively. This indicates to a certain extent better solubility of N in the CoCrFeMnNi fcc matrix in comparison with, for example, carbon [22,25,29]. Specifically, the equilibrium carbon solubility at 800 °C in fcc CoCrFeMnNi is believed to be < 0.1 at% [22]. Coupled with a strong solid solution strengthening effect of N [49], this opens opportunities to obtain an enhanced mechanical performance of the alloys, as will be discussed later. Note, however, that the phases found after annealing can correspond not to (fully) equilibrium condition due to the relatively short annealing time used. Note also that the obtained results on the N solubility in the CoCrFeMnNi strongly disagree with

Table 4
Room temperature mechanical properties of the CoCrFeMnNi alloys with different nitrogen concentrations (x) after cold rolling (CR) and annealing at different temperatures.

	YS, MPa	UTS, MPa	UE, %	TE, %
x = 0.5				
CR	1212	1329	1.5	15
700 °C	579	864	36	57
800 °C	464	798	40	58
900 °C	326	702	44	65
1000 °C	248	638	47	69
x = 1.0				
CR	1299	1442	1.2	14
700 °C	604	894	33	45
800 °C	539	900	39	56
900 °C	453	852	41	60
1000 °C	336	770	48	66
x = 2.0				
CR	1487	1640	1.5	9
700 °C	985	1195	12	16
800 °C	726	1020	18	24
900 °C	673	1021	30	47
1000 °C	570	988	29	42

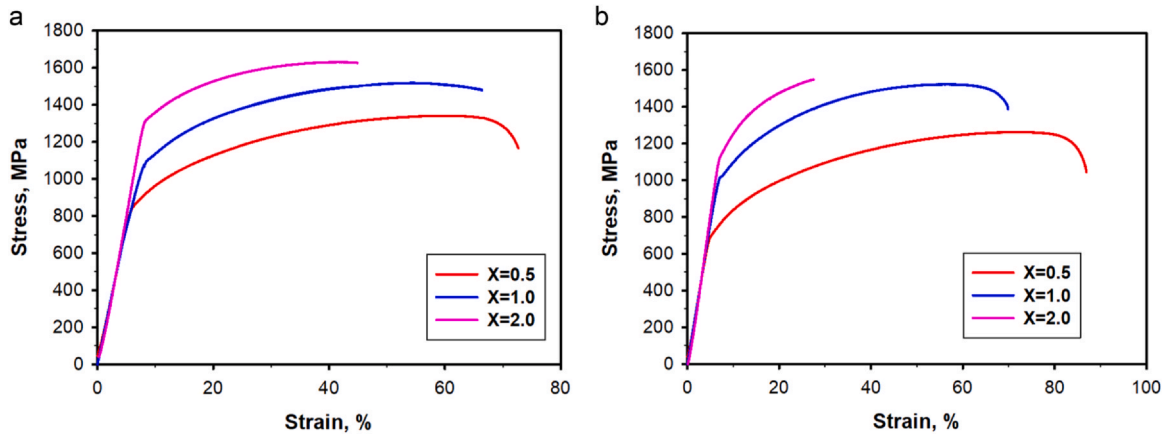

Fig. 7. Tensile stress-strain curves of the CoCrFeMnNi alloys with different nitrogen concentrations (x) after cold rolling and annealing at 800 °C (a) and 900 °C (a) obtained at 77 K.

Table 5
Mechanical properties of the CoCrFeMnNi alloys with different nitrogen concentrations (x) after cold rolling and annealing at 800 and 900 °C at 77 K.

Annealing temperature	YS, MPa	UTS, MPa	UE, %	TE, %
800 °C				
x = 0.5	782	1341	52	65
x = 1.0	1057	1504	43	57
x = 2.0	1286	1630	32	35
900 °C				
x = 0.5	661	1262	64	80
x = 1.0	1007	1522	47	61
x = 2.0	1097	1548	18	18

the Thermo-Calc predictions [46], probably due to well-known imperfections of the available databases [47].

The amount of nitrogen added to the CoCrFeMnNi alloy influenced on the development of recrystallization, both in terms of the recrystallization temperature and size of recrystallized grains. For example, a fully recrystallized microstructure was observed in the x = 0.5 alloy after annealing at 700 °C, while only 15% of recrystallized fraction were found in the x = 2.0 alloy. This effect appears to be associated with the presence of nitrogen in the solid solution rather than the nitrides precipitation. A strong interaction of interstitial solutes with grain boundaries and the formation of solute atmospheres, impedes the migration of grain boundaries, thereby providing a higher energy barrier for recovery and recrystallization during annealing [48]. The nitrides precipitation was observed to occur simultaneously with recrystallization (Fig. 4, for example), most probably because of mass transfer is needed for the particle growth. Similar observations were made for carbon-doped CoCrFeMnNi HEAs [25,38].

Another effect of the nitrogen doping was associated with a smaller fcc recrystallized grain size, especially in the x = 2.0 alloy (Fig. 3). Most likely, the precipitation of nitrides restricted grain growth in the fcc matrix. The slower kinetics of grain growth due to the particles' pinning effect can be expressed as per Zener's original equation [49]:

$$D_Z = a\frac{2d}{3F_v} \quad (1)$$

where D_z is the Zener limiting grain size, α is a scaling factor, d and F_v are the size and fraction of particles, respectively. The relationship between the experimental fcc grain size and particle size/fraction ratio in the x = 1.0 and x = 2.0 alloys (Table 2) after annealing at 700–1000 °C (700–900 °C in the x = 1.0 alloy because no nitrides were found in the x = 1.0 alloy after annealing at 1000 °C) is plotted in Fig. 10.

A linear dependence between the grain size and the particle size/particle fraction ratio (Fig. 10) confirms that the fcc grain growth was largely controlled by the Zener drag mechanism in the x = 1.0 and x = 2.0 alloys. The slope of the curves is almost identical for both alloys, yet the resulting grain size is much higher in the x = 2.0 alloy (see the two dots highlighted with the red oval in Fig. 10). This is most probably because the dots correspond to different annealing temperatures - 700°C and 1000°C for the x = 1.0 and x = 2.0 alloys, respectively. Thus, the mobility of the fcc grain boundaries and the size of recrystallized grains will be higher despite a similar slope and particle size/particle fraction ratio.

The mechanical properties of the alloys also demonstrated a strong dependence on both chemical composition and annealing temperature. For example, the strength has increased in proportion with the nitrogen content and decreased with an increase in the annealing temperature. Multiple strengthening mechanisms can operate in the program alloys, namely interstitial solid solution hardening, work hardening (in the alloys with partially recrystallized structure), grain boundary strengthening, and precipitation strengthening. However, the analysis performed earlier for the fine-grain carbon-doped CoCrFeMnNi-type alloys [35,44] revealed that the dominant strengthening mechanism is grain boundary strengthening. Therefore, we have plotted the yield strength of the alloys at 293 K in different conditions against the grain size ($D^{-0.5}$). Note that data for the x = 2.0 alloy after annealing at 700 °C was excluded from the analysis since the alloy was almost fully unrecrystallized. The obtained dependence is shown in Fig. 11.

It is apparent from Fig. 11 that a linear relationship between the yield strength and $D^{-0.5}$ is observed. It is the indication that the grain boundary strengthening is (mostly) responsible for the variations in the strength depending on the nitrogen content and annealing temperature. Note, however, that the nitride particles can effectively pin the fcc matrix grain boundaries (Fig. 10). Thus, the nitrides also contribute to strengthening, but in an indirect way [50,51].

According to Fig. 11, the Hall-Petch equation can be written as:

$$YS = \sigma_0 + k_{HP} * D^{-0.5} \quad (2)$$

Where YS is the yield strength, σ_0 is the friction stress, k_{HP} is the Hall-Petch coefficient, and D is the grain size. The results obtained (Fig. 11) suggest the σ_0 and k_{HP} values of 186 MPa and 650 MPa/μm$^{0.5}$, respectively.

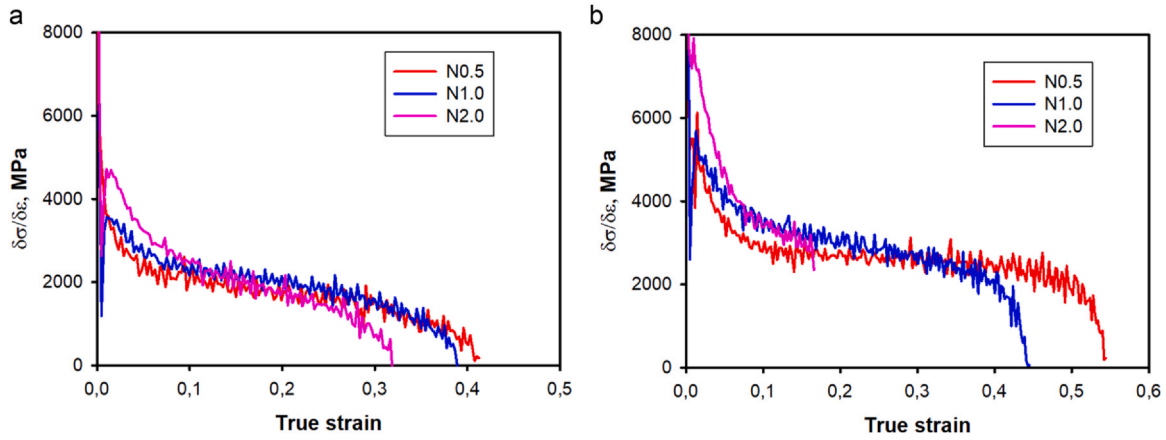

Fig. 8. Strain hardening curves of the CoCrFeMnNi alloys with different nitrogen concentrations (x) after cold rolling and annealing at 900 °C obtained at 293 K (a) and 77 K (b).

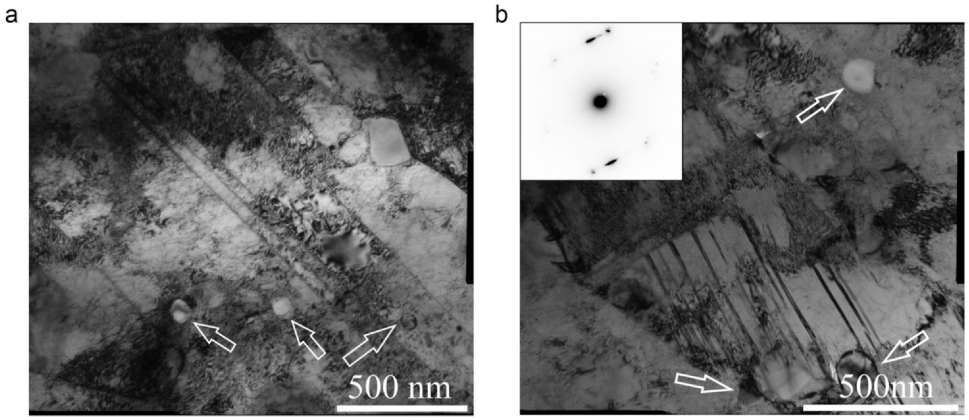

Fig. 9. TEM bright-field images of the CoCrFeMnNi alloy with x = 2.0 after cold rolling and annealing at 900 °C after tensile strain of 15% at 293 K (a) and 77 K (b). Some M_2N particles are marked with arrows.

The obtained k_{HP} value is somewhat higher than the data reported for the "pure" CoCrFeMnNi alloy – 494–497 MPa/μm$^{0.5}$ [3,52]. Note that much higher values of k_{HP} were reported for some doped CoCrFe(Mn)Ni, for example 935 MPa/μm$^{0.5}$ in the CoCrFeMnNi-1C alloy [27] or 824 MPa/μm$^{0.5}$ in the $Al_{0.3}$CoCrFeNi [53]. Thus, some increase in the Hall-Petch coefficient in the N-doped program alloys is not surprising.

Meanwhile, the reported σ_0 value for the undoped CoCrFeMnNi alloy is considerably lower – 125 MPa [3] than the value obtained in the present study (186 MPa). This discrepancy can be attributed to

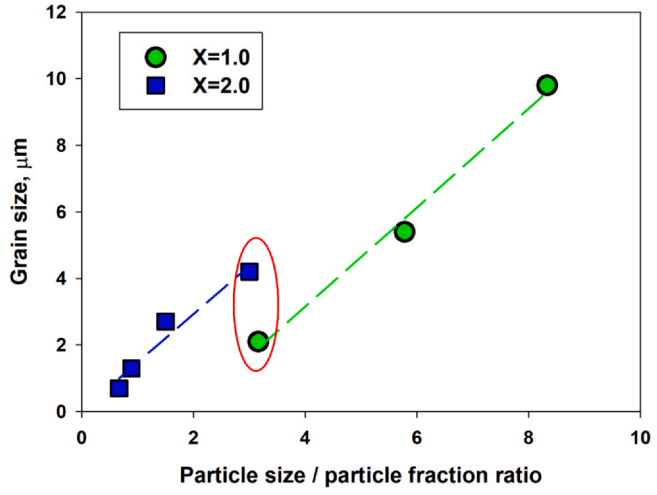

Fig. 10. Dependence of the fcc grain size on the particles size/fraction ratio in the CoCrFeMnNi alloy with 1.0 at% and 2.0 at% N. The dashed lines are only guides to eyes.

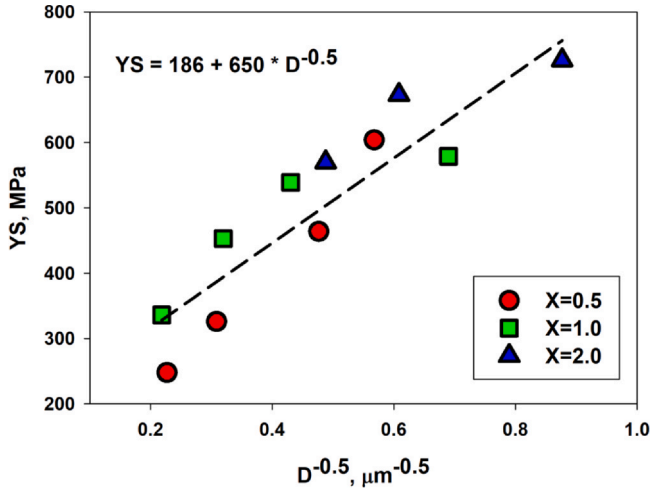

Fig. 11. Hall-Petch relationship for the program alloys at 293 K.

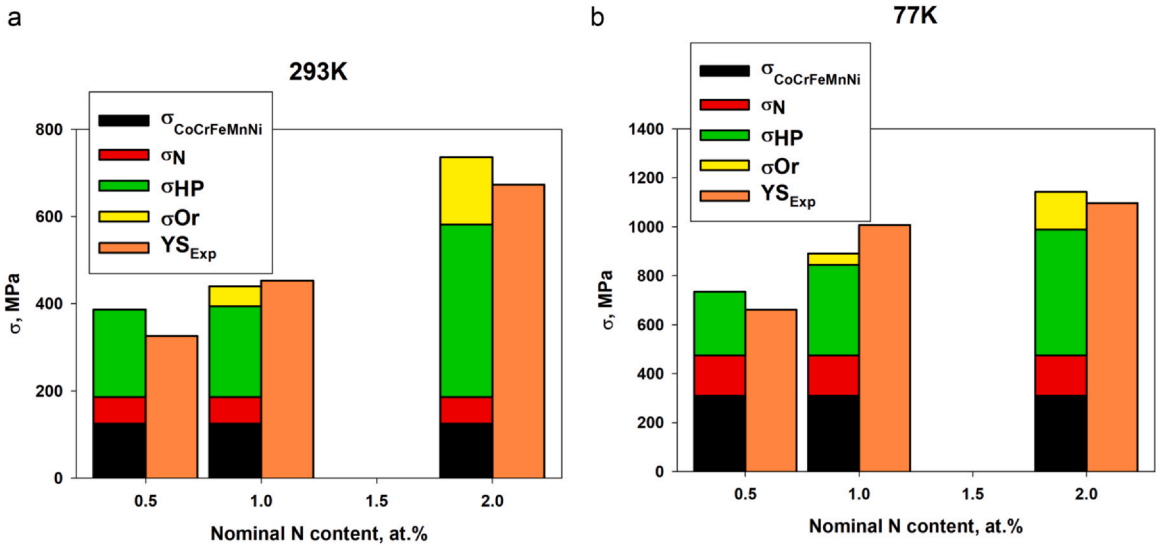

Fig. 12. Strengthening mechanisms operating in the program alloys after annealing at 900 °C at 293 K (a) and 77 K (b).

the fact that some nitrogen remains solved in the fcc matrix of the program alloys and causes interstitial strengthening [43]. In this case, the σ_0 value can be expressed as:

$$\sigma_0 = \sigma_{CoCrFeMnNi} + \sigma_N \quad (3)$$

Where $\sigma_{CoCrFeMnNi}$ is the friction stress of the undoped CoCrFeMnNi, and σ_N is the interstitial solid solution strengthening, which can be expressed as:

$$\sigma_N = k_N * C_N \quad (4)$$

Where k_N is the solid solution strengthening coefficient (117 MPa/at% at 293 K [43]), and C_N is the percentage of N solved in the fcc matrix. The absence of the nitrides in the x = 0.5 alloy suggests that C_N is at least 0.5 at% N. The value of σ_0, calculated using Eqs. (3) and (4) and values of $\sigma_{CoCrFeMnNi}$, k_N, and C_N listed above, is 183.5 MPa, which is almost identical to the experimental σ_0 value of 186 MPa (Fig. 11).

To gain additional insights into strengthening of the program alloys, we have performed a more detailed analysis of the strengthening mechanisms of the alloy annealed at 900 °C because of a more comprehensively studied structure (e.g., by TEM (Fig. 5)) and the availability of the mechanical behavior at 77 K (Fig. 7). In addition to grain boundary strengthening and interstitial solid solution strengthening, addressed above, the nitride particles can also provide strengthening per the Orowan mechanism [54]:

$$\sigma_{Or} = (0.538\, G\, b\, f^{1/2} / d)\, ln\, (d/2b) \quad (5)$$

where, $b = 2.58 \times 10^{-10}$ m^{-10} is the Burgers vector, $G = 80$ GPa is the shear modulus [2], f and d are the particles fraction and size (Table 3), respectively.

Thus, the overall strength of the program alloys can be expressed as following:

$$YS = \sigma_{CoCrFeNiMn} + \sigma_N + \sigma_{HP} + \sigma_{Or} \quad (6)$$

or.

$$YS = \sigma_{CoCrFeNiMn} + k_N * C_N + k_{HP}\, D^{-0.5} + (0{\cdot}538\, G\, b\, f^{1/2} / d)\, ln\, (d/2b) \quad (7)$$

The results of the different strengthening mechanisms contributions calculated using Eq. (7) were compared with the experimental yield strength (YS_{Exp}) of the alloys at 293 K at 77 K in Fig. 12a. A reasonable fit between the calculated and experimental data was observed. Moreover, the provided analysis has confirmed that grain boundary strengthening plays the dominant role among the considered strengthening mechanisms.

Further, we have tried to extend our analysis of the strengthening mechanisms of the program alloys to 77 K. Note that although an increase in strength of the fcc HEAs at cryogenic conditions has been reported numerous times [5], the qualitative analysis of such increase has never been performed to the best of the authors' knowledge. We have repeated calculations using Eq. (7) for the case of 77 K, using somewhat different parameters: $\sigma_{CoCrFeMnNi} = 310$ MPa [3] and $k_N = 316$ MPa/at% [49]. Besides, the Hall-Petch coefficient, k_{HP}, was also increased by 30% to 845 MPa/μm$^{0.5}$ per the results reported earlier for undoped CoCrFeMnNi [52]. We have also assumed that the Orowan strengthening is not changing with a decrease in temperature towards the cryogenic region. The results of calculations are shown in Fig. 12b. Again, a reasonable correlation between the experimental and predicted data was found. The obtained results suggest that an increase in strength due to a decrease in temperature from 293 K to 77 K can mostly be attributed to increased lattice friction of the CoCrFeMnNi matrix and interstitial solid solution strengthening.

Finally, the program alloys mostly demonstrated a typical strength-ductility trade-off at 293 K, i.e. become more ductile at the expense of strength (Table 4). That is, the alloys became more ductile with an increase in annealing temperature and a decrease in the N content. A decrease in testing temperature to 77 K results in some increment in ductility of the x = 0.5 and x = 1.0 alloys (Tables 4 and 5), similar to the majority of fcc HEAs [58]. An increase in ductility occurred simultaneously with an increase in strength, most possibly due to an enhanced strain hardening capacity (Fig. 8).

Meanwhile, the x = 2.0 alloy had noticeably lower ductility at cryogenic temperature (Tables 4 and 5). A similar decrease in ductility was observed in the as-cast x = 2.0 earlier, although the as-cast alloy exhibited even lower ductility (uniform elongation ~ 4%) and fractured in a brittle manner [43]. Some increment in ductility can be attributed to the activation of mechanical twinning in the thermomechanically processed alloy (Fig. 9b), while twinning was absent in the as-cast alloy [43]. It has been shown recently by ab initio calculations that N in an fcc CoCrFeMnNi solid solution increases stacking fault energy (SFE) [55], thus most probably suppressing mechanical twinning. The partitioning of N in the M_2N particles should therefore lower SFE and (possibly) activate mechanical twinning. However, future in-depth studies are still required to

verify the role of N on deformation mechanisms and mechanical properties of the fcc solid solution CoCrFeMnNi alloys.

In summary, the presented results demonstrate that a variety of different microstructures and mechanical properties can be obtained depending on the chemistry, i.e. nitrogen content, and processing conditions. It was revealed that fine-grained nitrogen-doped alloys can have an excellent strength ductility synergy, especially at cryogenic conditions, thus proving the potential of such materials for cryogenic applications in aerospace, marine shipbuilding, and natural gas industries [56].

5. Conclusions

In this study, structure and tensile properties of the CoCrFeMnNi high entropy alloy doped with different amounts of N (0.5–2.0 at%) after cold rolling to 80% thickness reduction and annealing at 700–1000℃ for 1 h were studied. The following conclusions were drawn:

1) A lamellar heavily deformed microstructure with a high dislocation density and some shear bands was observed in the program alloys after cold rolling. The nitrogen content has not qualitatively affected the deformed microstructure. The cold-rolled alloys had high strength (yield strength of ~1200–1500 MPa) but limited ductility (9–15%).
2) Annealing of the cold-rolled alloys has resulted in (i) the development of recrystallization in the fcc matrix of the alloys and (ii) precipitation of M_2N type nitrides in the alloys with 1.0 and 2.0 at % N. The amount of N has affected the recrystallization temperature. For example, after annealing at 700 °C the alloy with 0.5 at% was fully recrystallized, while the alloy with 2.0% was almost completely (85%) unrecrystallized. The fully recrystallized structure in the alloy with 2.0 at% N was obtained only after annealing at 900 °C. Besides, the fcc grain size was considerably smaller in the alloy with 2.0 at% N; for instance, the grain size was ~10 μm and ~3 μm in alloys with 0.5–1.0 and 2.0 at% N after annealing at 900 °C, respectively. Refinement of the fcc grain size was attributed to the pinning effect of the M_2N particles.
3) The annealed alloys have demonstrated a typical strength-ductility trade-off at 293 K, i.e. the alloys became more ductile with an increase in annealing temperature and a decrease in the N content. The quantitative analysis of the strengthening mechanisms has revealed that the grain boundary strengthening provides the highest contribution at 293 K. A decrease in the testing temperature to 77 K has resulted in a considerable increase in strength of the annealed alloys. Ductility of the alloys with 0.5–1.0 at% increased in cryogenic conditions, while the alloy with 2.0 at% N had lower ductility at 77 K than that at 293 K. The performed analysis suggested that the increase in strength at 77 K is mostly associated with the lattice friction and interstitial solid solution hardening.

CRediT authorship contribution statement

A. Semenyuk: Investigation, Writing – review & editing, Visualization, Supervision. **M. Klimova:** Investigation. **D. Shaysultanov:** Investigation. **G. Salishchev:** Conceptualization. **S. Zherebtsov:** Methodology, Writing – review & editing. **N. Stepanov:** Writing – original draft, Visualization, Supervision, Funding acquisition.

Declaration of Competing Interest

The authors declare that they have no known competing financial interests or personal relationships that could have appeared to influence the work reported in this paper.

Acknowledgments

The authors gratefully acknowledge the financial support from the Russian Science Foundation Grant No. 18-19-00003. The authors are grateful to the personnel of the Joint Research Center, "Technology and Materials", and Ms. Elizaveta Povolyava, Belgorod State University, for their assistance with the instrumental analysis.

References

[1] J.W. Yeh, S.K. Chen, S.J. Lin, J.Y. Gan, T.S. Chin, T.T. Shun, C.H. Tsau, S.Y. Chang, Nanostructured high-entropy alloys with multiple principal elements: novel alloy design concepts and outcomes, Adv. Eng. Mater. 6 (2004), https://doi.org/10.1002/adem.200300567 299-303+274.
[2] Z. Wu, H. Bei, G.M. Pharr, E.P. George, Temperature dependence of the mechanical properties of equiatomic solid solution alloys with face-centered cubic crystal structures, Acta Mater. 81 (2014), https://doi.org/10.1016/j.actamat.2014.08.026
[3] F. Otto, A. Dlouhý, C. Somsen, H. Bei, G. Eggeler, E.P. George, The influences of temperature and microstructure on the tensile properties of a CoCrFeMnNi high-entropy alloy, Acta Mater. 61 (2013) 5743–5755, https://doi.org/10.1016/j.actamat.2013.06.018
[4] C. Zhu, Z.P. Lu, T.G. Nieh, Incipient plasticity and dislocation nucleation of FeCoCrNiMn high-entropy alloy, Acta Mater. 61 (2013) 2993–3001, https://doi.org/10.1016/j.actamat.2013.01.059
[5] Z. Li, K.G. Pradeep, Y. Deng, D. Raabe, C.C. Tasan, Metastable high-entropy dual-phase alloys overcome the strength–ductility trade-off, Nature 534 (2016) 227–230, https://doi.org/10.1038/nature17981
[6] O.N. Senkov, G.B. Wilks, D.B. Miracle, C.P. Chuang, P.K. Liaw, Refractory high-entropy alloys, Intermetallics 18 (2010) 1758–1765, https://doi.org/10.1016/j.intermet.2010.05.014
[7] N.D. Stepanov, N.Y. Yurchenko, D.V. Skibin, M.A. Tikhonovsky, G.A. Salishchev, Structure and mechanical properties of the $AlCr_xNbTiV$ (x = 0, 0.5, 1, 1.5) high entropy alloys, J. Alloy. Compd. 652 (2015) 266–280, https://doi.org/10.1016/j.jallcom.2015.08.224
[8] N. Yurchenko, E. Panina, M. Tikhonovsky, G. Salishchev, S. Zherebtsov, N. Stepanov, Structure and mechanical properties of an in situ refractory $Al_{20}Cr_{10}Nb_{15}Ti_{20}V_{25}Zr_{10}$ high entropy alloy composite, 264 (2020) 127372, https://doi.org/10.1016/j.matlet.2020.127372
[9] B. Cantor, I.T.H. Chang, P. Knight, A.J.B. Vincent, Microstructural development in equiatomic multicomponent alloys, Mater. Sci. Eng. A 375 (2004) 213–218, https://doi.org/10.1016/j.msea.2003.10.257
[10] F. Otto, Y. Yang, H. Bei, E.P.P. George, Relative effects of enthalpy and entropy on the phase stability of equiatomic high-entropy alloys, Acta Mater. 61 (2013) 2628–2638, https://doi.org/10.1016/j.actamat.2013.01.042
[11] M.V. Klimova, D.G. Shaysultanov, S.V. Zherebtsov, N.D. Stepanov, Effect of second phase particles on mechanical properties and grain growth in a CoCrFeMnNi high entropy alloy, Mater. Sci. Eng. A 748 (2019) 228–235, https://doi.org/10.1016/J.MSEA.2019.01.112
[12] B. Schuh, F. Mendez-Martin, B. Völker, E.P. George, H. Clemens, R. Pippan, A. Hohenwarter, Mechanical properties, microstructure and thermal stability of a nanocrystalline CoCrFeMnNi high-entropy alloy after severe plastic deformation, Acta Mater. 96 (2015) 258–268, https://doi.org/10.1016/j.actamat.2015.06.025
[13] B. Gludovatz, A. Hohenwarter, D. Catoor, E.H. Chang, E.P. George, R.O. Ritchie, A fracture-resistant high-entropy alloy for cryogenic applications, Science 345 (2014) 1153–1158, https://doi.org/10.1126/science.1254581
[14] B. Gludovatz, A. Hohenwarter, K.V.S. Thurston, H. Bei, Z. Wu, E.P. George, R.O. Ritchie, Exceptional damage-tolerance of a medium-entropy alloy CrCoNi at cryogenic temperatures, Nat. Commun. (2016), https://doi.org/10.1038/ncomms10602
[15] Z. Zhang, M.M. Mao, J. Wang, B. Gludovatz, Z. Zhang, S.X. Mao, E.P. George, Q. Yu, R.O. Ritchie, Nanoscale origins of the damage tolerance of the high-entropy alloy CrMnFeCoNi, Nat. Commun. 6 (2015) 10143, https://doi.org/10.1038/ncomms10143
[16] Y.O. Kuzminova, D.G. Firsov, S.A. Dagesyan, S.D. Konev, S.N. Sergeev, A.P. Zhilyaev, M. Kawasaki, I.S. Akhatov, S.A. Evlashin, Fatigue behavior of additive manufactured CrFeCoNi medium-entropy alloy, J. Alloy. Compd. 863 (2021) 158609, https://doi.org/10.1016/j.jallcom.2021.158609
[17] Y. Kuzminova, D. Firsov, A. Dudin, S. Sergeev, A. Zhilyaev, A. Dyakov, A. Chupeeva, A. Alekseev, D. Martynov, I. Akhatov, S. Evlashin, The effect of the parameters of the powder bed fusion process on the microstructure and mechanical properties of CrFeCoNi medium-entropy alloys, Intermetallics 116 (2020) 106651, https://doi.org/10.1016/j.intermet.2019.106651
[18] A. Gali, E.P. George, Tensile properties of high- and medium-entropy alloys, Intermetallics 39 (2013) 74–78, https://doi.org/10.1016/j.intermet.2013.03.018
[19] I. Baker, Interstitials in f.c.c. high entropy alloys, Metals 10 (2020) 695, https://doi.org/10.3390/met10050695
[20] E. Astafurova, E. Melnikov, S. Astafurov, K. Reunova, M. Panchenko, V. Moskvina, I. Tumbusova, A comparative study of a solid solution hardening in carbon-alloyed $FeMnCrNiCo_{0.95}C_{0.05}$ high-entropy alloy subjected to different thermal-mechanical treatments, Mater. Lett. 285 (2021) 129073, https://doi.org/10.1016/j.matlet.2020.129073

[21] Z. Wang, I. Baker, Interstitial strengthening of a f.c.c. FeNiMnAlCr high entropy alloy, Mater. Lett. 186 (2016) 153–156, https://doi.org/10.1016/j.matlet.2016.05.122

[22] N.D. Stepanov, N.Y. Yurchenko, M.A. Tikhonovsky, G.A. Salishchev, Effect of carbon content and annealing on structure and hardness of the CoCrFeNiMn-based high entropy alloys, J. Alloy. Compd. 687 (2016) 59–71, https://doi.org/10.1016/j.jallcom.2016.06.103

[23] Z. Li, C.C. Tasan, H. Springer, B. Gault, D. Raabe, Interstitial atoms enable joint twinning and transformation induced plasticity in strong and ductile high-entropy alloys, Sci. Rep. 7 (2017) 40704, https://doi.org/10.1038/srep40704

[24] Z. Wang, I. Baker, W. Guo, J.D. Poplawsky, The effect of carbon on the microstructures, mechanical properties, and deformation mechanisms of thermomechanically treated $Fe_{40.4}Ni_{11.3}Mn_{34.8}Al_{7.5}Cr_6$ high entropy alloys, Acta Mater. 126 (2017) 346–360, https://doi.org/10.1016/j.actamat.2016.12.074

[25] Z. Li, Interstitial equiatomic CoCrFeMnNi high-entropy alloys: carbon content, microstructure, and compositional homogeneity effects on deformation behavior, Acta Mater. 164 (2019) 400–412, https://doi.org/10.1016/j.actamat.2018.10.050

[26] J. Peng, Z. Li, L. Fu, X. Ji, Z. Pang, A. Shan, Carbide precipitation strengthening in fine-grained carbon-doped FeCoCrNiMn high entropy alloy, J. Alloy. Compd. (2019), https://doi.org/10.1016/j.jallcom.2019.06.204

[27] N.D. Stepanov, D.G. Shaysultanov, R.S. Chernichenko, N.Y. Yurchenko, S.V. Zherebtsov, M.A. Tikhonovsky, G.A. Salishchev, Effect of thermomechanical processing on microstructure and mechanical properties of the carbon-containing CoCrFeNiMn high entropy alloy, J. Alloy. Compd. 693 (2017) 394–405, https://doi.org/10.1016/j.jallcom.2016.09.208

[28] M. Klimova, N. Stepanov, D. Shaysultanov, R. Chernichenko, N. Yurchenko, V. Sanin, S. Zherebtsov, Microstructure and mechanical properties evolution of the Al, C-containing CoCrFeNiMn-type high-entropy alloy during cold rolling, Materials (2017) 53, https://doi.org/10.3390/ma11010053

[29] M.V. Klimova, D.G. Shaysultanov, R.S. Chernichenko, V.N. Sanin, N.D. Stepanov, S.V. Zherebtsov, A.N. Belyakov, Recrystallized microstructures and mechanical properties of a C-containing CoCrFeNiMn-type high-entropy alloy, Mater. Sci. Eng. A 740–741 (2019) 201–210, https://doi.org/10.1016/j.msea.2018.09.113

[30] D. Shaysultanov, N. Stepanov, S. Malopheyev, I. Vysotskiy, V. Sanin, S. Mironov, R. Kaibyshev, G. Salishchev, S. Zherebtsov, Friction stir welding of a carbon-doped CoCrFeNiMn high-entropy alloy, Mater. Charact. 145 (2018) 353–361, https://doi.org/10.1016/j.matchar.2018.08.063

[31] H. Cheng, H.Y. Wang, Y.C. Xie, Q.H. Tang, P.Q. Dai, Controllable fabrication of a carbide-containing FeCoCrNiMn high-entropy alloy: microstructure and mechanical properties, Mater. Sci. Technol. 33 (2017) 2032–2039, https://doi.org/10.1080/02670836.2017.1342367

[32] I. Moravcik, J. Cizek, L. Gouvea, J. Cupera, I. Guban, I. Dlouhy, Nitrogen interstitial alloying of CoCrFeMnNi high entropy alloy through reactive powder milling, Entropy 21 (2019) 363, https://doi.org/10.3390/e21040363

[33] E.G. Astafurova, M.Y. Panchenko, K.A. Reunova, A.S. Mikhno, V.A. Moskvina, E.V. Melnikov, S.V. Astafurov, H.J. Maier, The effect of nitrogen alloying on hydrogen-assisted plastic deformation and fracture in FeMnNiCoCr high-entropy alloys, Scr. Mater. 194 (2021) 113642, https://doi.org/10.1016/j.scriptamat.2020.113642

[34] F. Xiong, R. Fu, Y. Li, D. Sang, Effects of nitrogen alloying and friction stir processing on the microstructures and mechanical properties of CoCrFeMnNi high-entropy alloys, J. Alloy. Compd. 822 (2020) 153512, https://doi.org/10.1016/j.jallcom.2019.153512

[35] Y. Han, H. Li, H. Feng, K. Li, Y. Tian, Z. Jiang, Enhancing the strength and ductility of CoCrFeMnNi high-entropy alloy by nitrogen addition, Mater. Sci. Eng. A 789 (2020) 139587, https://doi.org/10.1016/j.msea.2020.139587

[36] S.J. Sun, Y.Z. Tian, H.R. Lin, X.G. Dong, Y.H. Wang, Z.J. Zhang, Z.F. Zhang, Enhanced strength and ductility of bulk CoCrFeMnNi high entropy alloy having fully recrystallized ultrafine-grained structure, Mater. Des. 133 (2017) 122–127.

[37] S.J. Sun, Y.Z. Tian, X.H. An, H.R. Lin, J.W. Wang, Z.F. Zhang, Ultrahigh cryogenic strength and exceptional ductility in ultrafine-grained CoCrFeMnNi high-entropy alloy with fully recrystallized structure, Mater. Today Nano 4 (2018) 46–53, https://doi.org/10.1016/j.mtnano.2018.12.002

[38] M. Klimova, D. Shaysultanov, A. Semenyuk, S. Zherebtsov, N. Stepanov, Effect of carbon on recrystallised microstructures and properties of CoCrFeMnNi-type high-entropy alloys, J. Alloy. Compd. 851 (2021) 156839, https://doi.org/10.1016/j.jallcom.2020.156839

[39] D.E. Jodi, J. Park, N. Park, Strengthening of ultrafine-grained equiatomic CoCrFeMnNi high-entropy alloy by nitrogen addition, Mater. Lett. (2019) 126772, https://doi.org/10.1016/j.matlet.2019.126772

[40] D.E. Jodi, J. Park, B. Straumal, N. Park, Investigation on the precipitate formation and behavior in nitrogen-containing equiatomic CoCrFeMnNi high-entropy alloy, Mater. Lett. 258 (2020) 126806, https://doi.org/10.1016/j.matlet.2019.126806

[41] Y. Han, H. Li, H. Feng, Y. Tian, Z. Jiang, T. He, Mechanism of dislocation evolution during plastic deformation of nitrogen-doped CoCrFeMnNi high-entropy alloy, Mater. Sci. Eng. A (2021) 141235, https://doi.org/10.1016/j.msea.2021.141235

[42] I. Moravcik, H. Hadraba, L. Lim, I. Dlouhy, D. Raabe, Z. Li, Yield strength increase of a CoCrNi medium entropy alloy by interstitial nitrogen doping at maintained ductility, Scr. Mater. 178 (2020) 391–397, https://doi.org/10.1016/j.scriptamat.2019.12.007

[43] M. Klimova, D. Shaysultanov, A. Semenyuk, S. Zherebtsov, G. Salishchev, N. Stepanov, Effect of nitrogen on mechanical properties of CoCrFeMnNi high entropy alloy room and cryogenic temperatures, J. Alloy. Compd. 849 (2020) 156633, https://doi.org/10.1016/j.jallcom.2020.156633

[44] F. Xiong, R. Fu, Y. Li, B. Xu, X. Qi, Influences of nitrogen alloying on microstructural evolution and tensile properties of CoCrFeMnNi high-entropy alloy treated by cold-rolling and subsequent annealing, Mater. Sci. Eng. A 787 (2020) 139472, https://doi.org/10.1016/j.msea.2020.139472

[45] K.S. Chung, P.M. Yiu, T.F. Hung, C.H. Shek, Strengthening and deformation mechanism of a $Fe_{20}Co_{20}Cr_{20}Mn_{20}Ni_{20}$ high entropy alloy with high nitrogen content, J. Alloy. Compd. 871 (2021) 159587, https://doi.org/10.1016/j.jallcom.2021.159587

[46] A. Semenyuk, M. Klimova, S. Zherebtsov, N. Stepanov, Effect of interstitial elements on the cryogenic mechanical behavior of FCC high entropy alloys, Mater. Sci. 1016 (2021) 1386–1391, https://doi.org/10.4028/www.scientific.net/MSF.1016.1386

[47] S. Gorsse, O.N. Senkov, About the reliability of CALPHAD predictions in multicomponent systems, Entropy MDPI 20 (2018) 899, https://doi.org/10.3390/e20120899

[48] F.J. Humphreys, M. Hatherly, Recrystallization and Related Annealing Phenomena, Elsevier, 2004.

[49] E. Nes, N. Ryum, O. Hunderi, On the Zener drag, Acta Metall. 33 (1985) 11–22, https://doi.org/10.1016/0001-6160(85)90214-7

[50] Z. Wang, A. Genc, I. Baker, Direct versus indirect particle strengthening in a strong, ductile FeNiMnAlTi high entropy alloy, Mater. Charact. 132 (2017) 156–161, https://doi.org/10.1016/j.matchar.2017.08.019

[51] N.D. Stepanov, D.G. Shaysultanov, R.S. Chernichenko, D.M. Ikornikov, V.N. Sanin, S.V. Zherebtsov, Mechanical properties of a new high entropy alloy with a duplex ultra-fine grained structure, Mater. Sci. Eng. A 728 (2018) 54–62, https://doi.org/10.1016/j.msea.2018.04.118

[52] S.J. Sun, Y.Z. Tian, H.R. Lin, X.G. Dong, Y.H. Wang, Z.J. Wang, Z.F. Zhang, Temperature dependence of the Hall–Petch relationship in CoCrFeMnNi high-entropy alloy, J. Alloy. Compd. 806 (2019) 992–998, https://doi.org/10.1016/j.jallcom.2019.07.357

[53] B. Gwalani, V. Soni, M. Lee, S. Mantri, Y. Ren, R. Banerjee, Optimizing the coupled effects of Hall-Petch and precipitation strengthening in a $Al_{0.3}$CoCrFeNi high entropy alloy, 121 (2017) 254–260, https://doi.org/10.1016/j.matdes.2017.02.072

[54] T. Gladman, Precipitation hardening in metals, Mater. Sci. Technol. 15 (1999) 30–36, https://doi.org/10.1179/026708399773002782

[55] Y. Ikeda, F. Körmann, Impact of N on the stacking fault energy and phase stability of FCC CrMnFeCoNi: an ab initio study, J. Phase Equilib. Diffus. (2021), https://doi.org/10.1007/s11669-021-00877-x

[56] J.W. Bae, J.B. Seol, J. Moon, S.S. Sohn, M.J. Jang, H.Y. Um, B.-J. Lee, H.S. Kim, Exceptional phase-transformation strengthening of ferrous medium-entropy alloys at cryogenic temperatures, Acta Mater. 161 (2018) 388–399, https://doi.org/10.1016/j.actamat.2018.09.057